HiLL PUBLISHING

Scientific Access, 2025, 1(1), 27-31
https://www.hillpublisher.com/journals/sa/
ISSN Online: ****-****

Microstructure and Mechanical Properties of TiB_2/Al-Zn-Mg-Cu Composite Fabricated by Electron Beam Freeform[1]

Yi Gao[1], Xiaodong Li[2], Bin Yang[1], Yun Zhao[2], Xianfeng Li[1,*]

[1]School of Materials Science & Engineering, Shanghai Jiao Tong University, Shanghai 200240, China.
[2]Machinery Manufacturing Co., Ltd. of KSEC, Kunming 650217, Yunnan, China.

How to cite this paper: Yi Gao, Xiaodong Li, Bin Yang, Yun Zhao, Xianfeng Li. (2025) Microstructure and Mechanical Properties of TiB2/Al-Zn-Mg-Cu Composite Fabricated by Electron Beam Freeform. *Scientific Access*, 1(1), 27-31.
DOI: 10.26855/sa.2025.06.005

Received: April 30, 2025
Accepted: May 29, 2025
Published: June 27, 2025

***Corresponding author:** Xianfeng Li, School of Materials Science & Engineering, Shanghai Jiao Tong University, Shanghai 200240, China.

Abstract

Electron beam freeform fabrication (EBF[3]) is attracting more and more attention from researchers due to its suitability for space environments. In this paper, we report the microstructure and mechanical properties of a TiB_2/Al-Zn-Mg-Cu composite manufactured by EBF[3]. The main phases were α-Al and TiB_2 particles. There were equiaxed grains in the composite, and the average grain size distribution ranged from 17.3μm to 22.2μm. The cross-sectional microhardness exhibits an overall increasing distribution from 66 to 128 HV1 from the substrate to the top of the part. It had 360 MPa ultimate tensile strength, 216 MPa yield strength, and 16% elongation in the horizontal direction.

Keywords

Electron beam freeform fabrication; Aluminum matrix composites; Microstructure; Mechanical properties

Al-Zn-Mg-Cu aluminum alloys are widely used in the aviation and military industries due to their high specific strength, hardness, and fatigue resistance [1, 2]. In electron beam freeform fabrication (EBF3), an electron beam is used as a heat source to deposit molten metal onto a substrate or previously deposited layers [3-5]. The working environment of EBF3 is close to that of space, so it is more suitable for space environments than other additive manufacturing methods. Recently, researchers have devoted themselves to studying and implementing this method on titanium alloys and Al-Cu alloys [6, 7].

Taminger et al. [8] revealed the potential of microstructural control by accelerating voltage in EBF3 2219 aluminum alloy. Cui et al. [9] demonstrated the advantages of EBF3 technology in obtaining fully equiaxed grains, reducing element segregation, and inhibiting cracks. Lei et al. [10] studied the microstructure and mechanical properties of EBF3 TiB2/ZL205 thin-walled components. Bian et al. [11] successfully used the electron beam melting (EBM) process to refine the grain size of Al-Si alloy, thereby improving its tensile ductility.

However, there are few studies on the feasibility, microstructure, or mechanical properties of TiB2/Al-Zn-Mg-Cu composites prepared by EBF3. In this study, in-situ self-generated TiB2/Al-Zn-Mg-Cu welding wire was additively manufactured into TiB2/Al-Zn-Mg-Cu composite thin-walled components by EBF3 technology, and its microstructure and mechanical properties were tested and analyzed.

1. Experimental Materials and Methods

In this experiment, a 1.2 mm diameter TiB2/Al-Zn-Mg-Cu composite welding wire was selected as the filler material. The wire was obtained by the mixed salt method and then drawn into a TiB2/Al-Zn-Mg-Cu composite ingot. The

[1] The Chinese version of this paper has been published in the *International Journal of Materials Science*. This version is a translated version and has been authorized and approved for publication by two publishers.

EBF3 preparation process was carried out using Zcomplex X3 under vacuum conditions (about 7.6×10-2 Pa). The selected heat source was an electron beam; the current was 40 mA, and the frequency was 300 Hz. The wire feeding speed and the travel speed remained unchanged, at 3.2 m/min and 500 mm/min, respectively. Table 1 shows the chemical composition of the wire and the material at different positions of the prepared EBF3 component.

Table 1. Chemical composition of TiB_2/Al-Zn-Mg-Cu wire and EBF[3] components at different locations (wt.%)

Compositions	Zn	Mg	Cu	Cr	Si	Fe	Ti	B	Al
Wire	5.740	2.500	1.650	0.220	0.027	0.012	2.640	1.150	Bal.
SH1	1.150	0.905	1.722	0.282	0.029	0.189	2.591	1.171	Bal.
SH2	2.347	1.666	1.832	0.237	0.026	0.013	2.624	1.149	Bal.
SH3	2.062	1.543	1.732	0.240	0.025	0.013	2.598	1.171	Bal.
SH4	1.696	1.296	1.766	0.243	0.024	0.012	2.638	1.200	Bal.

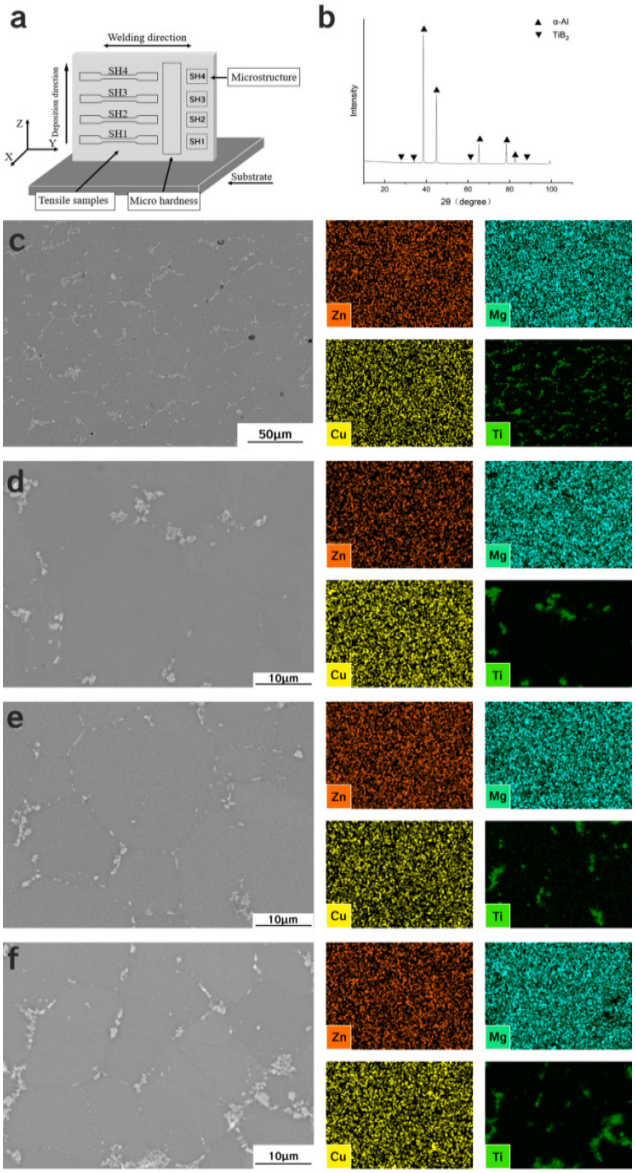

Figure 1. (a) Schematic diagram of sampling at different positions; (b) XRD results of TiB_2/Al-Zn-Mg-Cu composites prepared by EBF[3]; (c)-(f) SEM results: (c) SH1; (d) SH2; (e) SH3; (f) SH4.

After the EBF3 component was prepared, the metallographic specimens and tensile specimens were cut by a wire-cutting electrospark machine at the positions shown in Figure 1(a). The phase composition of the specimens at different positions was analyzed by X-ray diffractometer (XRD) and energy dispersive spectroscopy (EDS). The porosity test of the sample was carried out on a laboratory high-resolution X-ray microtomography (XCT) system. The microstructure was observed using a TESCAN scanning electron microscope (SEM) equipped with an electron backscatter diffraction (EBSD) detector. The hardness test of the sample was carried out using an HVS-30P Vickers hardness tester with a load of 10 kg and a loading time of 15 s. The tensile test was carried out in strain control mode with a tensile speed of 1×10-3 s^{-1}.

2. Experimental Results and Discussion

2.1 Microstructure

From the EDS spectrum and XRD data in Figure 1, it can be clearly seen that there is almost no segregation of alloy elements, and only a very small amount of phase is observed at the grain boundaries. This phenomenon is due to the vacuum environment of EBF^3 and its slow heat dissipation characteristics, which together promote the reduction of thermal stress and the suppression of element segregation [5, 8]. Further observation shows that TiB_2 is evenly distributed along the grain boundaries of aluminum.

As shown in Figure 2, the XCT scan results clearly show the distribution of micropores from the bottom to the top of the EBF^3-TiB_2/Al-Zn-Mg-Cu composite. In the bottom layer, the porosity remains at a low 0.2%. However, as the deposition height increases, a small number of unevenly distributed macropores begin to appear, causing the porosity to increase significantly to about 4.7%. These pores are mainly concentrated near the molten pool boundary, and overall, the porosity increases with the increase in deposition height. In the figure, the dark area represents a lower density, while the bright area indicates a higher alloying element content and better material properties. In addition, the contrast changes in Figure 2 are consistent with the data in Table 1, further confirming the observations of the pore distribution. Bounded by the molten pool boundary, the area with dense pores visually presents a lighter tone, which is in sharp contrast to the dense part. This phenomenon provides a certain degree of explanation for the hardness fluctuations shown in Figure 4(a).

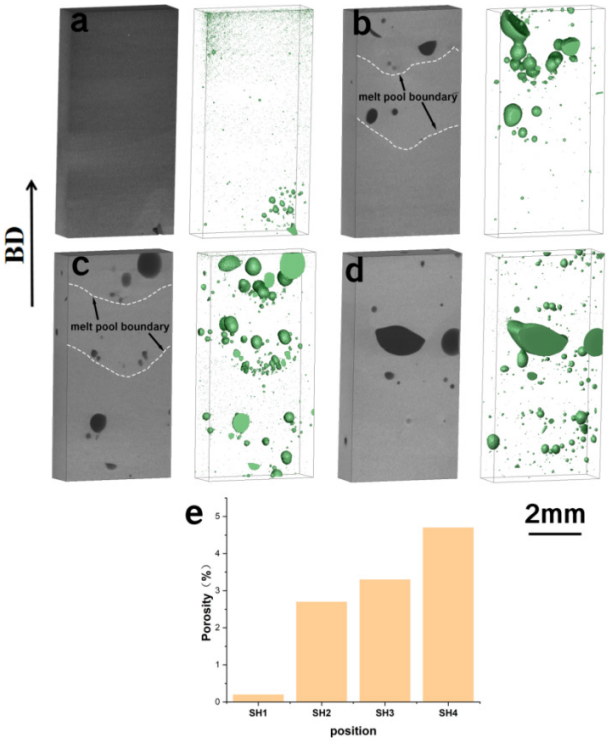

Figure 2. (a)-(d) XCT results: (a) SH1; (b) SH2; (c) SH3; (d) SH4; (e) Porosity at different locations.

Figure 3 shows the IPF diagram of the TiB_2/Al-Zn-Mg-Cu composite material and its grain size distribution statistics. It can be clearly seen from the figure that the grains present a uniform equiaxed crystal morphology. During the deposition process, as each layer is stacked and cooled, heat is effectively transferred from the previous layer to the next layer, providing a preheating effect for the next layer. This preheating mechanism significantly reduces the temperature gradient and constructs a cyclic thermal field environment, which leads to the coarsening of the grains in the middle area of the printed part (specifically, the grain size of the SH1 layer is 17.3 μm, the SH2 layer is 20.7 μm, and the SH3 layer is 22.2 μm) [12]. In contrast, since the top layer undergoes fewer thermal cycles and can hardly produce a significant in-situ heat treatment (IHT) effect, its grain size is relatively small, only 18.9 μm.

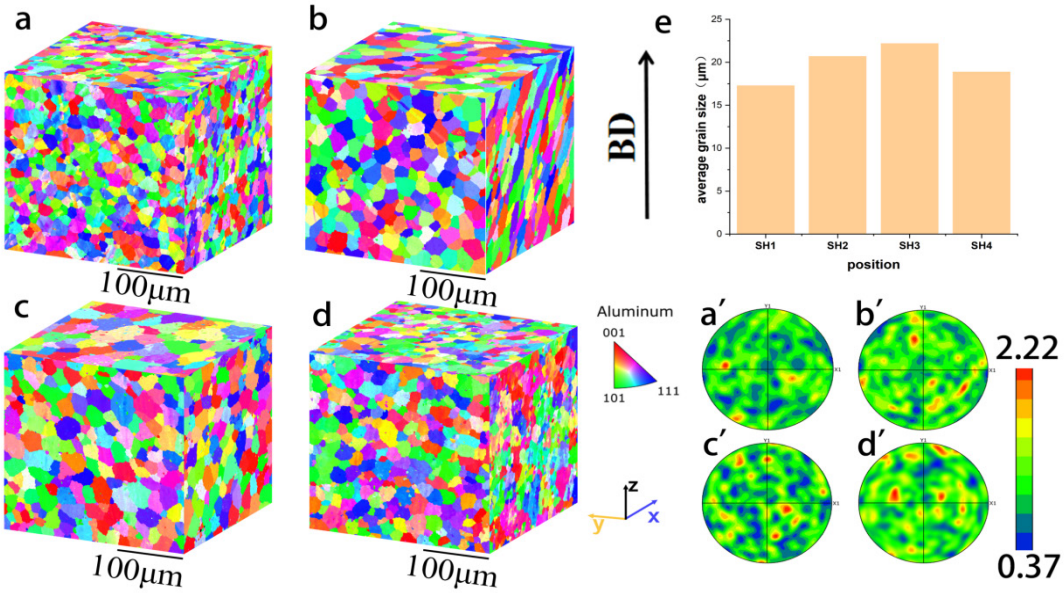

Figure 3. (a)-(d) IPF, (a')-(d') pole figures: (a) SH1; (b) SH2; (c) SH3; (d) SH4; (e) grain size at different positions.

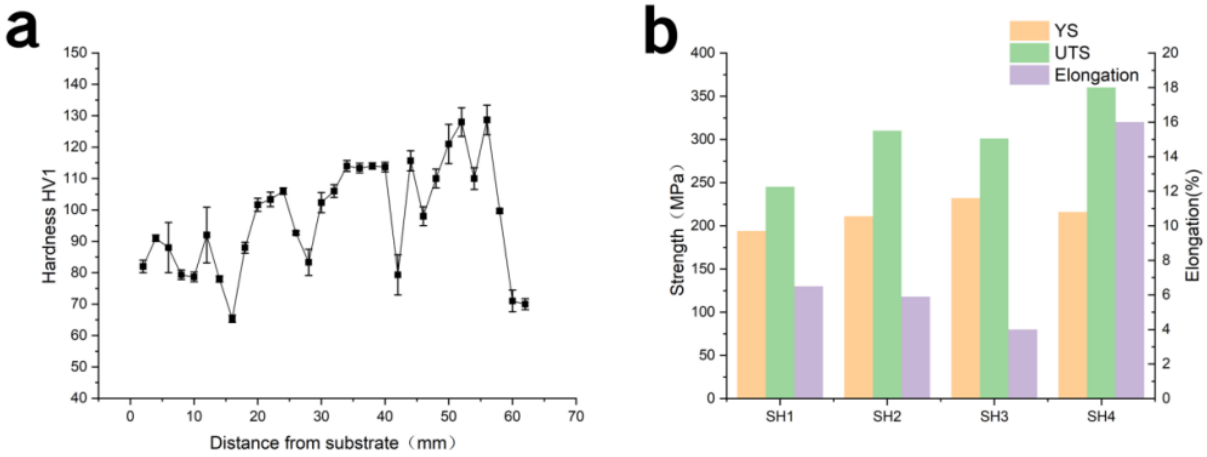

Figure 4. (a) Hardness distribution along the building direction; (b) Tensile properties at different locations.

2.2 Mechanical properties

Figure 4(a) shows the distribution of hardness. It can be seen that during the test, the hardness values of the EBF^3-TiB_2/Al-Zn-Mg-Cu composites showed significant differences between multiple test points, ranging from 66 HV to 128.7 HV. From the bottom to the top of the cross section, the hardness showed a clear upward trend, and the strength gradually increased. It is worth noting that although the grains in the bottom layer are finer than those in the middle, the content of alloy elements in this area contributes more significantly to the hardness. In addition, through the

variance analysis of the elongation between different samples, we found that the degree of variation was statistically significant ($p<0.05$), which indicates that the uneven distribution of porosity may have a significant effect on the plastic deformation ability of the material. To further verify this, we used XCT technology to reconstruct the pore distribution of the sample in three dimensions, as shown in Figure 2. The results show that the pores are mainly concentrated near the boundary of the deposition layer, and the porosity shows an upward trend with the increase of deposition height. Figure 4(b) shows the tensile properties at different locations. It can be seen that the average yield strength and ultimate tensile strength of SH4 are 216 MPa and 360 MPa, which are 11.3% and 46.9% higher than those of SH1, respectively, showing a significant strengthening effect.

3. Conclusion

(1) For the TiB_2/Al-Zn-Mg-Cu composites prepared by EBF^3, the main phases are composed of α-Al and TiB_2, among which the TiB_2 particles are mostly distributed along the grain boundaries.
(2) The grains of EBF^3-TiB_2/Al-Zn-Mg-Cu composite materials are mainly equiaxed grains. The grain size increases first and then decreases from the bottom to the top. Among them, the minimum grain size is 17.3 μm, and the maximum grain size is 22.2 μm.
(3) The hardness of the EBF^3-TiB_2/Al-Zn-Mg-Cu composites shows an increasing trend with the increase of deposition height, from 66 HV to 128 HV, which corresponds to the distribution of alloying elements.
(4) The average yield strength and ultimate tensile strength of the top SH4 of the EBF^3 component are 216 MPa and 360 MPa, which are 11.3% and 46.9% higher than those of the bottom SH1, respectively.

References

[1] Sha G, Cerezo A. Early-stage precipitation in Al-Zn-Mg-Cu alloy (7050). Acta Mater. 2004;52(15):4503-16.

[2] Buha J, Lumley RN, Crosky AG. Secondary ageing in an aluminium alloy 7050. Mater Sci Eng A. 2008;492(1-2):1-10.

[3] Yan W, Yue Z, Feng J. Study on the role of deposition path in electron beam freeform fabrication process. Rapid Prototyp J. 2017;23:1057-68.

[4] Filippov AV, Fortuna SV, Gurianov DA, et al. On the problem of formation of articles with specified properties by the method of electron beam freeform fabrication. J Phys Conf Ser. 2018;1115:042044.

[5] Watson JK, Taminger KM, Hafley RA, et al. Development of a prototype low-voltage electron beam freeform fabrication system. Sci Tech Aerosp Rep. 2003;41(5).

[6] Li Z, Cui Y, Wang L, et al. An investigation into Ti-22Al-25Nb in-situ fabricated by electron beam freeform fabrication with an innovative twin-wire parallel feeding method. Addit Manuf. 2022;50:102552.

[7] Xu J, Zhu J, Fan J, et al. Microstructure and mechanical properties of Ti-6Al-4V alloy fabricated using electron beam freeform fabrication. Vacuum. 2019;167:364-73.

[8] Taminger KM, Hafley RA, Domack MS. Evolution and control of 2219 aluminium microstructural features through electron beam freeform fabrication. Mater Sci Forum. 2006;519-521:1297-302.

[9] Cui R, Wang L, Yao L, et al. On the solidification behaviors of AlCu5MnCdVA alloy in electron beam freeform fabrication: microstructural evolution, Cu segregation and cracking resistance. Addit Manuf. 2022;51:102606.

[10] Lei S, Li X, Deng Y, et al. Microstructure and mechanical properties of electron beam freeform fabricated TiB2/Al-Cu composite. Mater Lett. 2020;277:128273.

[11] Bian H, Aoyagi K, Zhao Y, et al. Microstructure refinement for superior ductility of Al-Si alloy by electron beam melting. Addit Manuf. 2020;32:100982.

[12] Moritz S, Schwanekamp T, Reuber M, et al. Impact of in situ heat treatment effects during laser-based powder bed fusion of 1.3343 high-speed steel with preheating temperatures up to 700°C. Steel Res Int. 2023;94(6):2200775.